ATMOSPHERIC PLASMA SPRAYING COATINGS FROM ALUMINA–TITANIA FEEDSTOCK COMPRISING BIMODAL PARTICLE SIZE DISTRIBUTIONS

Mónica Vicent [a,*], Emilie Bannier [a], Rodrigo Moreno [b], Mª Dolores Salvador [c], Enrique Sánchez [a]

[a] Instituto de Tecnología Cerámica (ITC), Asociación de Investigación de las Industrias Cerámicas (AICE), Universitat Jaume I (UJI), Castellón, Spain

[b] Instituto de Cerámica y Vidrio (ICV), Consejo Superior de Investigaciones Científicas (CSIC), Madrid, Spain

[c] Instituto de Tecnología de Materiales (ITM), Universidad Politécnica de Valencia (UPV), Valencia, Spain

Abstract

In this work, Al_2O_3 –13 wt% TiO_2 submicron-nanostructured powders were deposited using atmospheric plasma spraying. The feedstocks were obtained by spray drying two starting suspensions of different solids content, prepared by adding nanosized TiO_2 and submicron-sized Al_2O_3 powders to water. The spray-dried granules were heat-treated to reduce their porosity and the powders were fully characterised in both untreated and thermally treated state.Comparison with two commercial feedstocks was carried out. Characterisation allowed a temperature for the termal reatment to be chosen on the basis of the sprayability of the feedstock and the preservation as much as possible of the submicron-sized structure of the unfired agglomerates. Optimisation of the deposition conditions enabled the reconstituted powders to be successfully deposited, yielding coatings that were well bonded to the substrate. The coating microstructure, characterised by SEM, was mostly formed by a matrix of fully molten particles where the presence of semi-molten feedstock agglomerates was also observed. Moreover, microhardness, toughness, adhesion and tribological behaviours were determined, and the impact of the granule characteristics on these properties was studied. It was found that changing the feedstock characteristics allows controlling the coating quality and properties. In general, good mechanical properties were obtained using a feedstock comprising a binary mixture of submicrometric Al_2O_3 and nanometric TiO_2 particles in the spray-dried poder

1. Introduction

Thermal spray, and particularly atmospheric plasma spray (APS), is one of the most economical and viable processes to obtain coatings at an industrial scale, given its high deposition rates and that there is no need for special atmospheric or chemical chambers. Additional advantages are the durability and high thickness of the coatings. The manufacture of nanostructured coatings would provide enhanced properties over those obtained for micronic or submicronic ones. In order to obtain nanostructured coatings it is necessary to use nanoparticles (1) as raw material. However, nanoparticles need to be reconstituted to a sprayable size in order to use regular powder feeders as well as to provide a route to safe handling of nanoparticles.[1] Reconstitution generally takes place by spray drying of a nanoparticle suspension and, frequently, thermal treatment (partial sintering) of the resulting granules (2). Although many authors have addressed the role of slurry formulation on the characteristics of the ceramic granules and many others have obtained spray-dried powders for termal spraying, (3, 4) most papers using nanostructured spray-dried feedstock only mention the agglomeration process without providing a complete experimental study of nanoparticle suspension prepa ration, spray-drying operation, or thermal treatment of the resulting agglomerates. Thus, the correlation between agglomeration process variables, agglomerate characteristics, and coating microstructure and properties is far from being well established

Al_2O_3 –TiO_2 coatings fabricated with nanopowders show very promising bonding strength and wear resistance when compared with conventional feedstock as reported elsewhere (5, 6). Although many research efforts have been made to pass from the micro-scale to either the nano- or the submicron-scale using both powders or liquids as feedstock, (7, 8) few attempts have been made to use feedstocks in which mixtures of different particle size distributions, e.g. submicron–nano sized particles. The use of a bimodal distribution of submicron-nano particles, comprising the precursor suspension of the spray-dried pow- der, can give rise to significant benefits during the suspension processing, i.e. higher solids content and lower viscosity lead- ing to better properties in the resulting

feedstock agglomerates, such as higher agglomerate bulk density and improved pow- der flowability (9, 10). This is particularly interesting for alumina suspension due to the intrinsic difficulties associated with the preparation of concentrated nanoparticle suspensions of alu- mina as reported elsewhere (11). The relationship between these improved agglomerate feedstock characteristics and the final coating properties has been scarcely treated in the literatura (10).

In this respect, we have also recently reported improved photo- catalytic activity in APS TiO_2 coatings when using a mixture of nano and submicrometric particles in the spray-dried feedstock. Much higher density agglomerates were obtained which led to better properties in the final coatings (11, 12). In previous research by the authors, it was found that the nanostructured spray-dried agglomerates obtained from concen- trated $Al_2 O_3$ –13 wt% TiO_2 suspensions yielded coatings with lower void content than those obtained using powders from less concentrated suspensions (11). However, feedstocks made up of powders with bimodal particle size distribution (submi- cronic–nanometric particles) were not explored.

This work deals with the relationship between the reconstituted granule characteristics and the properties of $Al_2 O_3$ –13 wt% TiO_2 coatings obtained from spray-dried feedstocks made up of TiO_2 nanoparticles and $Al_2 O_3$ submicro- metric particles with a view to addressing the potential benefits of the use of bimodal feedstocks. Complete characterisation of feeding powders (FEG-ESEM, granule size distribution, flowa- bility and apparent density) and of newly developed coatings (microstructure by SEM and mechanical properties such as microhardness, toughness, wear and pull-off) was performed. The expected benefits of the use of submicron-sized alumina (instead of nanosized alumina) together with nanosized titania comprising the spray-dried feedstock can be then summarised as follows: easier suspension preparation and handling with the achievement of much higher solids concentration, better feedstock characteristics associated with an (expected) higher agglomerates density and much lower feedstock cost.

2. Experimental

2.1. Feedstock preparation and characterisation

The following commercial powders were used as starting materials: (1) a submicron-sized, high purity a -$Al2 O3$ (Condea-Ceralox HPA-0.5, Sasol, USA) with a mean particle size of 0.35 μm and a specific surface area of 9.5 m2/g; and (2) a nanosized TiO2 powder (Aeroxide® P25, Degussa-Evonik, Germany) with an average primary particle size of 40 nm, a specific surface area of 50 m2/g, and a relative ratio of anatase:rutile phases of 3:1 (13). Mixtures of submicronic alumina and nanometric titania were always prepared at a relative weight ratio of 87:13. Finally, and for comparison purposes, two comercial feedstocks with the same Al2O3:TiO2 weight ratio, were also deposited: a conventional microstructured one (Metco 130, Sulzer Metco, Germany), referred as MC, and a nanostructured one (NanoxTM S2613S, Inframat Advanced Materials, USA), referred as NC.

The colloidal stability of aqueous suspensions of the TiO2 nanopowder as well as the coarser alumina powder has been previously evaluated by zeta potential measurements (9). This information allowed choosing the most adequate nature and proportion of dispersant so as to subsequently prepare high solids content suspensions. Thus, concentrated suspensions were prepared to solid contents of 30 vol.% and 50 vol.% (i.e. at 67 and 80 wt%, respectively) using deionised water. A comercial polyacrylic acid-based polyelectrolyte (DURAMAXTM D-3005, Rohm & Haas, USA) was used as a deflocculant. This was supplied as an aqueous solution of polyacrylic acid (PAA) with 35 wt% active matter of PAA [(C3H4O2)n] and an average molecular weight of 2400. Studies elsewhere have shown that this deflocculant is suitable for obtaining concentrated suspensions of both studied material (13,14). The suspensions were prepared by adding first the PAA required to disperse all the particles (4 wt% PAA in relation to the titania content and 0.3 wt% PAA in relation to the alumina content). The foregoing PAA contents refer to the active matter concentration. After that, the titania nanopowder was added and homogenized with sonication for 1 min and subsequently the alumina powder was dispersed (without sonication). The mixture was then kept for 15 min under mechanical stirring.

It was not necessary to use a binder for spray-drying. In fact, spray-dried granules with adequate mechanical strength were obtained from the 30 vol.% and 50 vol.% suspensions (hereinafter feedstock AsTn30 and AsTn50, respectively) in a spray dryer (Mobile Minor, Gea Niro, Denmark) with a drying capacity of 7 kg water/h as set out elsewhere (11). Granule size distribution was measured by laser diffraction (Mastersizer, Malvern, UK). Agglomerate apparent density was calculated from powder tapped density by assuming a theoretical packing factor of 0.6, which is characteristic of monosize, spherical particles (15). Powder flowability was evaluated in terms of the Hausner ratio,

determined by dividing powder tapped density by powder apparent density (15).Free-flowing powders have a Hausner ratio <1.25.

In order to obtain denser granules, the spray-dried powders were heat treated in an electric kiln at a temperature rate of 25 °C/min to different maximum temperatures, which depended on the powder sample, with soaking time of 60 min (11). The main objective of the heat treatment is to enhance the mechanical strength of the agglomerates and to reduce their shell porosity meanwhile the submicro/nano-structure of the feedstock agglomerates should be preserved as much as posible (2, 11). A test was previously carried out in a hot stage microscope (Misura 3, Expert System Solutions, Italy) so as to ascertain the temperatura of this thermal treatment. The hot stage microscope is an instrument that allows the visualisation of a sample while it is being subjected to a heating cycle. At the same time, it allows the simple shape to be recorded on a computer throughout shrinkage. The recorded images enable the evolution of sample shrinkage to be determined as a function of temperature, by means of an image analysis instrument. The spray-dried sample was used to press a cylindrical button, 3 mm in diameter and 3 mm in height, which was placed on a support that was then set in the hot stage microscope sample holder, where it was subjected to a heating cycle at a rate of 25 ∘ C/min. The shrinkage–temperature curve was determined from the recorded images. Finally, pore structure was evaluated by mercury intrusión porosimetry, MIP (AutoPore IV 9500, Micromeritics, USA), crystalline phases in feedstock samples were identified by Xray diffraction technique (XRD D8 Advance, Bruker AXS, Germany) and a field-emission gun environmental scanning electron microscope, FEG-ESEM (QUANTA 200FEG, FEI Company, USA) was used to examine the microstructure of both untreated and thermally treated feedstocks.

2.2. Coating deposition

$Al_2 O_3 -13$ wt% TiO_2 coatings were deposited by APS on stainless steel substrates (AISI 304) prepared as set out elsewhere (16). The plasma spray system consisted of a gun (F4-MB, Sulzer Metco, Germany) operated by a robot (IRB 1400, ABB, Switzerland). Before spraying, the substrate was blasted with corundum grit and cleaned with ethanol to remove any dust or grease residue from the surface. After that, a Ni–Al metallic alloy (METCO 450NS, Sulzer Metco, Germany) was sprayed between steel substrate and ceramic coating in order to improve adhesion. Moreover, it was also necessary to hold the substrate temperature between 95 ∘ C and 200 ∘ C, before $Al_2 O_3 -13$ wt% TiO_2 deposition, in order to avoid spalling during the final cooling. Finally, the deposition was made using argon and hydrogen as plasma-forming gases. The same spraying conditions were used in all deposition experiments: Ar flow = 35 slpm, H_2 flow = 12 slpm, arc intensity = 600 A, spraying distance = 0.12 m and spraying velocity = 1 m/s.

2.3. Coating characterisation techniques

First, the coating microstructures were observed by SEM (JSM6300, JEOL, Japan). Coating porosity was evaluated by image analysis from ten backscattered electron mode micrographs at 1000 magnification. Crystalline phases in coating samples were also identified by X-ray diffraction technique. The hardness and fracture toughness of the section of coatings were determined using an indentation technique. A conventional diamond pyramid indenter (Vickers) was fit to the piece of equipment (4124, INNOVATEST, Netherlands) and a load of 3 N was applied for 15 s according to the standard specification ASTM E92-72. The fracture toughness was determined by measuring the radial crack length generated on the corners of the track produced as a consequence of the Vickers indentation test. A minimum of 10 tests were averaged for hardness and toughness determination. Wear tests were carried out under dry sliding conditions using a pin-on-disk tribometer (MT2/60/SCM/T, Microtest, Spain) in accordance with ASTM wear testing standard G99-03. As friction partner, 5 mm diameter- Si_3N_4 ball was used. The normal load, sliding speed and distance were fixed at 10 N, 0.1 m/s and 1000 m, respectively. Testing was carried out in air, at room temperature. Prior to measuring hardness, toughness and wear, the samples were polished (RotoPol-31, Struers, Denmark) with diamond to 1 μm roughness for hardness and toughness determination, and with SiC to 2–3 μm for wear tests. The pull-off tests were performed according to ASTM D4541 in a PosiTest (AT-A, DeFelsko, USA). The dolly, whose diameter was 10 mm, was attached to the coating surface with a curable epoxy adhesive for 8 h. After that, the dolly was vertically pulledoff (with a 2.0 MPa/s rate) while measuring the necessary force. The results are the average of 3 repeated tests done on each sample.

3. Results and discussion

3.1. Feed powder agglomeration process

A former study revealed that the conventional powder (MC) is formed by angular particles between 20 μm and 60 μm obtained by a fusing and crushing process while the nanostructured feedstock (NC) contained highly porous agglomerates with a granule mean size of 38 μm which were made up of nanoparticles with a size ranging 50–500 nm (16). Figure 1 shows FEG-ESEM micrographs of the as-spray-dried powders obtained from 30 vol.% and 50 vol.% suspensions at different magnifications (samples AsTn30 and AsTn50, respectively). The typical doughnut-shape morphology of spray-dried agglomerates is observed in most granules of both powders (11). However, the 50 vol.% poder shows coarser agglomerates as well as less amount of nonspherical, small agglomerates leading to a more homogeneous powder. This finding coincides with that observed for nanoparticle suspensions obtained with different solids content(11).Thus, as expected, stable, higher solids content suspensions give rise to larger agglomerates due to the higher suspension viscosity. Higher magnification of the solid areas of the agglomerates of both powders reveals that the granules are porous and formed by the agglomeration of the individual nano- and submicronsized particles. In both powders, coarser alumina particles are clearly visible together with the titania nanoparticles. In addition, denser particle arrangement is observed in the cross section of the AsTn50 powder granule as a result of the much larger number of particles in the stabilised starting suspensions.

Table 1 lists some properties of interest for spray-dried powders to be used as feedstock in plasma spraying: the Hausner ratio, which is related to the flowability of the powder and the agglomerate bulk density, which is directly related to its weight. Data of reference feedstock (samples MC and NC) are also included. According to the literature, (3, 17), relatively dense (higher than 1000 kg/m$_3$ apparent density) and free-flowing agglomerates are necessary for a suitable feeding into the plasma torch. In general, all the samples exhibit adequate characteristics to be used as APS powders. However, significant differences can be observed among these four samples (AsTn30, AsTn50, MC and NC). With regard to the agglomerate bulk density although the highest value is shown by the commercial sample MC, this is because this sample is a fused and crushed dense powder. Thus, no direct comparison can be done between this feedstock and the corresponding spray-dried powders. The agglomerate density of the two powders obtained in this research is much higher than that of the NC sample as a consequence of the better packing efficiency inside the agglomerate associated with the submicronic–nanometric particle arrangement (12). Moreover, the Hausner ratio for the three spray-dried powders was ≤ 1.25, indicating good flowability and confirming that they are appropriate for APS process. The higher value of this ratio (lower flowability) for the MC sample is due to the angular morphology of the particles comprising this powder.[16] Note that in the case of as-spray-dried powders, granule size distribution could not be measured by laser diffraction as they were broken during the measurement.

3.2. Thermal treatment of the spray-dried powders

Thermal treatment of the spray-dried powders commonly represents the second step of the reconstitution process for feedstock preparation in APS. In order to determine the beginning of the sintering process and thus to determine the heat treatment temperature, tests were conducted in a hot stage microscope. These tests were carried out on powder samples without any preliminary shaping or compaction of the powder and, thus, the results are actually representative of the feed powder behaviour and not of the sintering process of a given shaped sample or coupon. The evolution of powder shrinkage as a function of temperature is then plotted. Figure. 2 shows the shrinkage versus temperature curves for samples AsTn30 and AsTn50 together with the reference NC powder. As expected sample made up of nanoparticles (NC) displays much higher sintering rate evaluated from the slope of the shrinkage–temperature curve profile. On contrary, the sintering rate of the two other samples is more gradual as a consequence of the presence of submicrometric particle in the powder. Furthermore the role of the agglomerate bulk density (set out in Table 1) in the sintering process is of paramount significance. On the one hand, the higher the agglomerate density the lower the maximum shrinkage. In this way, the maximum sintering shrinkage of NC sample is almost twice that of the two other powders as a consequence of the much lower agglomerate density of the nanostructured feedstock (see Table 1). On the second hand, the decrease of the agglomerate density results in a delay in the initial sintering temperature. This last finding highlights the impact of the agglomerate density on the beginning of the sintering process. Samples made up of bimodal particle size distribution (submicrometric–nanometric sizes), which gave rise to higher agglomerate density (i.e. closer particle contact) lead to powders that show lower initial sintering temperatures than those of the NC feedstock despite this last sample is formed by nanoparticles.

Figure 3 shows the FEG-ESEM micrographs of thermally treated AsTn30 and AsTn50 samples. Similar micrographs for a nanostructured, spray-dried powder were previously reported (11). The evolution of the agglomerate microstructure is typical of a solid-state sintering process. This sintering process yields significant changes in sizes and shapes of grains and pores. Grain growth for both nano- and submicrometer-sized particles of the starting agglomerates is apparent at 1200 ºC as shown in the micrograph of AsTn30 sample. Thus, the sintering process

shown by the shrinkage–temperature curves takes place by means of a rapid grain growth of firstly titania nanoparticles and secondly alumina submicrometric particles.[9] In this way, submicron character of the particles which is visible at 1200 ºC for both powders has practically disappeared at 1235 ºC. Sintering process can also be followed by monitoring the evolution of the pore structure of the agglomerates. These measurements were directly done on powder sample, not on shaped samples. Pore sizing measurements are particularly intended to analyse the intragranular (fine size) porosity since the powder is fed into plasma torch without any consolidation (shaping) process. Figure 4 shows the pore size distribution curves obtained by mercury intrusion porosimetry for AsTn30 and AsTn50 untreated and thermally treated at 1235 ºC powders. The initial bimodal distribution of porosity is associated with large pores between granules (intergranular porosity, marked INTER in Figure 4) and small pores inside the agglomerates (intragranular porosity, marked INTRA in Figure 4). The intergranular porosity which largely depends of the sample preparation for porosimetry test shows scarce interest for APS process since the powder is fed into the plasma torch without any compacting effect. But the intragranular porosity allows the sintering effect to be estimated. It is worthwhile noticing that the void associated to the doughnut (toroid) morphology of the spray-dry agglomerates is mainly measured in the first step of Hg intrusion process, i.e. where the intergranular porosity is determined. Thus, as shown in this figure, the initial total porosity (maximum cumulative mercury intrusion volume) and the intragranular pore size (worked out from the INTRA portion of the pore size curve) are smaller for the as-spray-dried AsTn50 powder confirming the higher packing density of the agglomerates obtained from more concentrated suspensions. As the sintering process proceeds, the porosity decreases and the pore size increases as a consequence of the pore coarsening effect of the small pores.

Granule size distribution (Figure 5) confirmed some of the foregoing results. The AsTn50-1200ºC powder displayed a slightly coarser granule mean size than those of AsTn30-1200 ºC powder. It is generally recognised that thermal spray powders exhibit agglomerate size distributions ranging from 15 μm to 200 μm (2,18). The volumetric mean sizes were 57 μm and 110 μm (Table 1) and the volumetric quantities of 15 μm undersize agglomerates were only 2.0% and 3.5% for the 30 vol.% and 50 vol.% thermally treated samples, respectively. Thus, both powders fit well the average requirements. As mentioned above, the reconstitution process of APS feedstock aims to obtain sprayable, denser agglomerates in which the submicron-sized structure can be as much as possible preserved. As a consequence, the temperature chosen to increase the density was 1200 ◦C for both AsTn30 and AsTn50 samples (hereinafter AsTn30-1200 ◦C and AsTn50-1200 ◦C samples, respectively). The spray-dried powders were heat treated in an electric kiln with soaking time of 60 min at this given temperature. The agglomerate bulk density of the heat treated powders were 3100 kg/m3 and 3580 kg/m3 for the samples AsTn30 and AsTn50, respectively (Table 1). Despite this partial sintering process, the achieved density values of the thermally treated granules are still lower from those of the MC, fused and crushed grains (3830 kg/m3). With regard to the Hausner ratio or agglomerate size, the values of these parameters showed almost no variation with temperature (Table 1).

Finally, the XRD patterns of the untreated and AsTn30- 1200 ºC and AsTn50-1200 ºC samples revealed the following results. As set out in Section 2.1 , the untreated powder (either AsTn30 or AsTn50) is made up of α−Al2 O3 and mostly anatase. After heat treating most metastable anatase transforms into stable rutile. α−Al2 O3 remains as the stable phase for alumina. No formation of aluminum–titanate was identified due to the low temperature of the thermal treatment (9). The patterns of the untreated and thermally treated AsTn50-1200 ◦ºC powders are shown in Figure 6. Very similar patterns were obtained with AsTn30 powders.

With regard to reference powders MC and NC, in both cases aluminum oxide was found as corundum (α−Al2 O3), whereas titanium oxide was mainly composed of anatase with a low proportion of rutile. Concerning the commercial nanostructured powder, XRD analysis also confirmed the presence of some oxide additives (CeO2 in cerianite form and ZrO2 as zirconia and baddeleyite), (16).

3.3. Microstructure and phase distribution of the coatings

Four different types of coatings were obtained from the four spray-dried feedstocks (untreated AsTn30 and AsTn50 and heat treated AsTn30-1200 ºC and AsTn50-1200 ºC samples) by depositing all powders according to the spraying conditions set out in Section 2.2. This is because the objective of the work was to evaluate the influence of the characteristics of the different feedstocks on coatings microstructure and properties by keeping constant the (standard) plasma spraying conditions

Figure 7 shows SEM micrographs of these four coatings together with two representative micrographs of reference coatings (MC and NC) obtained with the same spraying conditions. The coatings microstructure is clearly influenced by the feedstock characteristics, as revealed by SEM observations (Figure 7). As expected, the coating obtained from

the conventional powder (MC) shows a typical splat-like microstructure, formed by successive impacts of fully molten droplets. However, the layers deposited from the nanostructured powder (NC) exhibit a bimodal microstructure formed by partially molten agglomerates that retained the initial nanostructure, surrounded by a fully molten matrix. Such microstructure has been extensively reported in the literatura (19, 20). Regarding coatings obtained from untreated and heat treated AsTn30 and AsTn50 samples, these coatings also displayed some few partially molten areas as observed in Figure 7, which are made of coarser particles than those comprising the partially molten areas of NC coating, as the feedstock mainly contained submicron particles. Yet, it has to be pointed out that these coatings are mainly formed by fully molten areas, as a consequence of the sintering grade and very low porosity of the initial granules. Thus, despite the nanostructured character of the primary particles comprising the comercial NC powder, the high porosity associated to these agglomerates results in coatings containing partially melted areas which preserve in some extent the starting nanostructure. On contrary, the much higher density of the submicrometric–nanometric feedstock diminishes the contribution of the initial agglomerate microstructure to the final coating microstructure. Figure 8 compares higher magnifications micrographs of the partially molten areas in NC and AsTn50-1200 ◦ C coatings. As it can be seen, partially molten areas in AsTn50-1200 ◦ C coating are made up of larger particles exhibiting less porous assembly.

The XRD patterns of the coatings are shown in Figure 9. Firstly, it can be seen that the coatings obtained from both thermally untreated powders mainly consist of α-Al$_2$O$_3$, α-Al$_2$O$_3$ and rutile. These findings are consistent with the phases observed in most of the works related to this Al$_2$O$_3$ –TiO$_2$ system which employ submicron or nanostructured feedstocks (18, 21). Secondly, on comparing coatings obtained from thermally treated powders with the coatings made from their corresponding untreated powders, the formers display a slightly higher amount of α-Al$_2$O$_3$ at the expense of α -Al$_2$O$_3$ which is probably related to the powder trajectory through the plasma torch as well as its melting stage. Finally, some minor phases were also observed, more specifically, there was a little Al$_2$TiO$_5$ formed in all the coatings (22), as well as some minor amounts of Magneli phases (Ti$_{in}$O$_{2n-1}$; $\mathbf{n}$ = 4–10).

Table 2 shows the porosity values obtained by SEM for all the coatings. Porosity data agree with the typical values observed in these types of coatings. However, some differences were also found between them. The coatings obtained from both comercial powders presented a lower porosity due to different reasons. On the one hand, the fused nature and small grain size of the MC sample. On the other hand, NC sample contains higher amount of smaller granules. Indeed, smaller granules are easier to melt, giving rise to more deformable droplets, and consequently to lower coating porosity (3, 18). Although this last statement could be inconsistent with the fact that NC coating showed a higher amount of partially molten areas, it should be taken into account that nano-scale porosity can hardly be evaluated by SEM technique. With regard to the feedstocks preparedin this work, thermal treatment results in coatings with slightly lower porosity, meanwhile no differences were observed between AsTn30 and AsTn50 powders. This is because, at this low range of coating porosities the contribution of the agglomerate density to the final coating porosity is negligible as compared with the contribution coming from the melting and subsequent deformation of the agglomerates during the deposition process. On the other hand, although some partially molten areas were identified by SEM, these areas could not be quantified owing to their low proportion in the coating. Finally, coatings thicknesses are also detailed in Table 2. As it can be seen, the lowest thickness was obtained with the commercial, fused and crushed feedstock.

3.4. Coating mechanical properties

Coatings mechanical properties (adhesion strength, Vickers microhardness, fracture toughness, and wear rate) for the four spray-dried feedstocks (untreated AsTn30 and AsTn50 and heat treated AsTn30-1200 ◦ C and AsTn50-1200 ºC) as well as for the two reference coatings (MC and NC) are shown in Figure 10 in terms of bar diagrams. As it can be seen, despite the differences in the characteristics of the feeding powders, the adhesión strength of all coatings showed similar values. However, nanostructured coating (NC) showed somehow lower fracture toughness than that of conventional and submicron–nanometric ones. Such results are apparently in contradiction with the common hypothesis of a crack deviation effect of the unmelted nanozones present throughout the bimodal microstructure (18, 19, 21) suggesting poor cohesion of these nanozones due to the low density of the granules found in the corresponding feedstock together with the plasma spraying conditions used in this work. As a consequence, cracks may propagate easily between the nanoparticles explaining the lower fracture toughness. With regard to the rest of feedstocks, higher values of toughness were obtained for the coatings deposited from the spray-dried powders prepared in this research. These values were even higher than that of the MC coating. A much better microstructural homogeneity of these coatings as set out above in comparison with the one sprayed from the nanostructured feedstock as well as the presence of fewer but denser partially molten areas can be the reason for such high values of toughness.

More interestingly, significant differences were observed in the microhardness of the coatings, which varied from 2.2 GPa, for the conventional layer, up to 9.5 GPa, for AsTn30-1200 ºC coating. Besides, it can be observed that when the microhardness increases, the wear resistance of the coating is improved. In fact, the best wear performance was found for AsTn30-1200 ºC coating while MC layer displayed the highest wear loss. Nanostructured coating (NC) shows an intermediate behaviour with a significantly higher wear resistance than that of the conventional layer.

The increased wear resistance of coatings obtained from nanostructured feedstocks in comparison with conventional (obtained from micrometric powders) coatings has been extensively reported in the recent literatura (10, 16, 18, 21). The reasons showed in the literature for explaining this behaviour are as follows: the toughening contribution of the partially molten nanostructured zones (18, 23, 24) (not seen in this work), a more homogeneous TiO_2 distribution inside the splats leading to higher splat bonding strength (5, 16) and the role of different additives such as CeO_2 and ZrO_2 added to the composition.[25] In this mentioned research, the effect of agglomerate size and size distribution of the feedstock on the final coating microstructure has also been pointed out (18, 26, 27).

As reported elsewhere, a feedstock with smaller agglomerates and a narrower agglomerate size distribution is preferred to produce dense coatings exhibiting well bonded, relatively dense nanostructured regions. All these works have focused on agglomerate size meanwhile the influence of the agglomerate density has been scarcely addressed. Bertrand et al. (28) showed that the combination of dense poder with large agglomerate size produces coatings with very high amount of unmolten areas in TiO_2 coatings whenever low energy spraying conditions were used. In fact, calculations with zirconia poder (29 have proven that dense (5680 kg/m^3) zirconia agglomerates, 50 μm in diameter, melt much more than porous (2840 kg/m3) due to the better heat propagation. Following all this research, in this work, we have shown that the use of high density spray-dried agglomerates in the feeding poder gives rise to low porosity coatings with a quite homogeneous microstructure leading to optimal mechanical properties. The way of obtaining such high density agglomerates was based on the use of a bimodal particle size distribution in the starting powder agglomerates with a significant amount of submicronsized particles instead of nanosized ones. The employment of submicron-sized particles makes it easy the processability of the spray-drying suspension allowing the preparation of high solids content suspensions. Although the findings obtained have been very promising, further research is still necessary so as to connect feedstock characteristics and coating microstructure and properties using the Al_2O_3 –TiO_2 system and/or other plasma spray techniques.

4. Conclusions

This study compares the microstructure and mechanical properties of Al_2O_3 –13 wt% TiO_2 APS coatings deposited from powders obtained by spray drying two starting suspensions of different solids content, prepared by adding nanosized TiO_2 and submicron-sized Al_2O_3 powders to water. The spray-dried granules were heat-treated to reduce their porosity. Thermal treatment temperature was chosen on the basis of the sintering behaviour of the feedstocks. The powders were fully characterised in both untreated and thermally treated state. Comparison with a conventional (microstructured) and a nanostructured comercial feedstock was carried out.

Despite the differences observed in the powders studied, in general, all the samples exhibit adequate characteristics in terms of granule bulk density and powder flowability so as to be used as APS powders. In particular, the use of highly concentrated suspensions containing a bimodal distribution (submicron- and nano-sized particles) leads to a spray-dried powder with the highest agglomerate density and good flowability. Thermal treatment was shown to be an efficient process for producing highly sinterable feedstock, yielding coatings with slightly lower porosity, independently of the solid concentration of the starting suspension used to obtain the reconstituted agglomerates.

 All coatings, except the conventional one, displayed a bimodal microstructure with partially molten agglomerates that retained the initial structure of the feedstock surrounded by a fully molten matrix. However, the amount of these partially molten areas is much higher in the case of the coating obtained from the nanostructured commercial powder which was constituted by highly porous agglomerates. In general, the coatings obtained from the submicron– nanometric reconstituted powders led to better mechanical properties than those of the coating obtained from the nanostructured feedstock whereas the conventional coatings displayed the worst wear behaviour. A much better microstructural homogeneity of these coatings in comparison with the one sprayed from the nanostructured feedstock, along with the presence of fewer but denser partially molten areas can be the reason for such enhanced

values of mechanical properties, particularly microhardness and wear resistance. Although the findings obtained are very promising, further research is still necessary so as to connect feedstock characteristics and coating microstructure and properties in this or other ceramic systems.

Acknowledgements

References

1. Faure B, Lindeløv JS, Wahlberg M, Adkins N, Jackson P, Bergström L. Spray drying of TiO$_2$ nanoparticles into redispersible granules. Powder Technol 2010;203(2):384–8.

2. Fauchais P, Montavon G, Lima RS, Marple BR. Engineering a new class of thermal spray nano-based microstructures from agglomerated nanostructured particles, suspensions and solutions: an invited review. J Phys D Appl Phys 2011;44:093001, http://dx.doi.org/10.1088/0022-3727/44/9/093001.

3. Fauchais P, Montavon G, Bertrand G. From powders to thermally sprayed coatings. J Therm Spray Technol 2010;19(1/2):56–80.

4. Berger-Keller N, Bertrand G, Filiare C, Meunier C, Coddet C. Microstructure of plasma-sprayed titania coatings deposited from spray-dried powder. Surf Coat Technol 2003;168(2/3):281–90.

5. Ahn J, Hwang B, Song EP, Lee S, Kim NJ. Correlation of microstructure and wear resistance of Al2O3–TiO2 coatings plasma sprayed with nanopowders. Metall Mater Trans A 2006;37(6):1851–61.

6. Lin X, Zeng Y, Lee SW, Ding C. Characterization of alumina–3 wt.% titania coating prepared by plasma spraying of nanostructured powders. J Eur Ceram Soc 2004;24(4):627–34.

7. Fauchais P, Vardelle M, Coudert JF, Vardelle A, Delbos C, Fazilleau J. Thermal plasma deposition from thick to thin coatings and from micro-to nanostructure. Pure Appl Chem 2005;77(2):475–85.

8. Darut G, Ageorges H, Denoirjean A, Montavon G, Fauchais P. Effect of the structural scale of plasma-sprayed alumina coatings on their friction coefficients. J Therm Spray Technol 2008;17(5/6): 788–95.

9. Molina T, Vicent M, Sánchez E, Moreno R. Dispersion and reaction sintering of alumina–titania mixtures. Mater Res Bull 2012;47:2469–74.

10. Vicent M, et al. Influence of the feedstock characteristics on the microstructure and properties of Al2O3–TiO2 plasma-sprayed coatings. Surf Coat Technol 2013;220:74–9.

11. Sánchez E, et al. Preparation and spray drying of Al2O3–TiO2 nanoparticle suspensions to obtain nanostructured coatings by APS. Surf Coat Technol 2010;205(4):987–92.

12. Bordes MC, et al. Microstructure and photocatalytic activity of APS coatings obtained from different TiO2 nanopowders. Surf Coat Technol 2013;220:179–86.

13. Vicent M, Sánchez E, Santacruz I, Moreno R. Dispersion of TiO2 nanopowders to obtain homogeneous nanostructured granules by spray-drying. J Eur Ceram Soc 2011;31(8):1413–9.

14. Gutiérrez CA, Moreno R. Preventing ageing on Al2O3 casting slips dispersed with polyelectrolytes. J Mater Sci 2000;35(23): 5867–72.

15. Amorós JL, Blasco A, Enrique JE, Negre F. Características de polvos cerámicos para prensado (Characteristics of ceramic powders for pressing). Bol Soc Esp Ceram Vidr 1987;26(1):31–7.

16. Sánchez E, et al. Deposition of Al2O3–TiO2 nanostructured powders by atmospheric plasma spraying. J Therm Spray Technol 2008;17(3): 329–37.

17. Cao XQ, Vassen R, Schwartz S, Jungen W, Tietz F, Stöever D. Spray-drying of ceramics for plasma-spray coating. J Eur Ceram Soc 2000;20(14/15):2433–9.

18. Marple BR, Lima RS. Engineering nanostructured thermal spray coatings: process–property–performance relationships of ceramic based materials. Adv Appl Ceram 2007;106(5):265–75.

19. Lima RS, Marple BR. Thermal spray coatings engineered from nanostructured ceramic agglomerated powders for structural, termal barrier and biomedical applications: a review. J Therm Spray Technol 2007;16(1):40–63.

20. Bansal P, Padture NP, Vasiliev A. Improved interfacial mechanical properties of Al2O3–13 wt% TiO2 plasma-sprayed coatings derived from nanocrystalline powders. Acta Mater 2003;51(10):2959–70.

21. Dejang N, Watcharapasorn A, Wirojupatump S, Niranatlumpong P, Jiansirisomboon S. Fabrication and properties of plasma-sprayed Al2O3/TiO2 composite coatings: a role of nano-sized TiO2 addition. Surf Coat Technol 2010;204(9-10):1651–7.

22. YangY. Wang Y, Wang Z, Liu G, Tian W. Preparation and sintering behaviour of nanostructured alumina/titania composite powders modified with nanodopants. Mat Sci Eng A 2008;490(1/2):457–64.

23. Luo H, Goberman D, Shaw L, Gell M. Indentation fracture behavior of plasma-sprayed nanostructured Al2O3–13 wt.% TiO2 coatings. Mater Sci Eng A 2003;346(1/2):237–45.

24. Song EP, Ahn J, Lee S, Kim NJ. Effects of critical plasma spray parameter and spray distance on wear resistance of Al2O3–8 wt.% TiO2 coatings plasma-sprayed with nanopowders. Surf Coat Technol 2008;202(15):3625–32.

25. Wang Y, Jiang S, Wang M, Wang S, Xiao TD, Strutt PR. Abrasive wear characteristics of plasma sprayed nanostructured alumina/titania coatings. Wear 2000;237(2):176–85.

26. Lima RS, Kucuk A, Berndt CC. Integrity of nanostructured partially stabilized zirconia after plasma spray processing. Mater Sci Eng A 2001;313(1/2):75–82.

27. Guo HB, Murakami H, Kuroda S. Effect of hollow spherical powder size distribution on porosity and segmentation cracks in thermal barrier coatings. J Am Ceram Soc 2006;89(12):3797–804.

28. Bertrand G, Berger-Keller N, Meunier C, Coddet C. Evaluation of metastable phase and microhardness on plasma sprayed titania coatings. Surf Coat Technol 2006;200(16/17):5013–9.

29. Ben-Ettouil F, Mazhorova O, Pateyron B, Ageorges H, El-Ganaoui M, Fauchais P. Predicting dynamic and thermal histories of agglomerated particles injected within a d.c. plasma jet. Surf Coat Technol 2008;202(18):4491–5.

Figure 1. FEG-ESEM micrographs of the as-spray-dried powders obtained from 30 vol.% and 50 vol.% suspensions at different magnifications (samples AsTn30 and AsTn50, respectively).
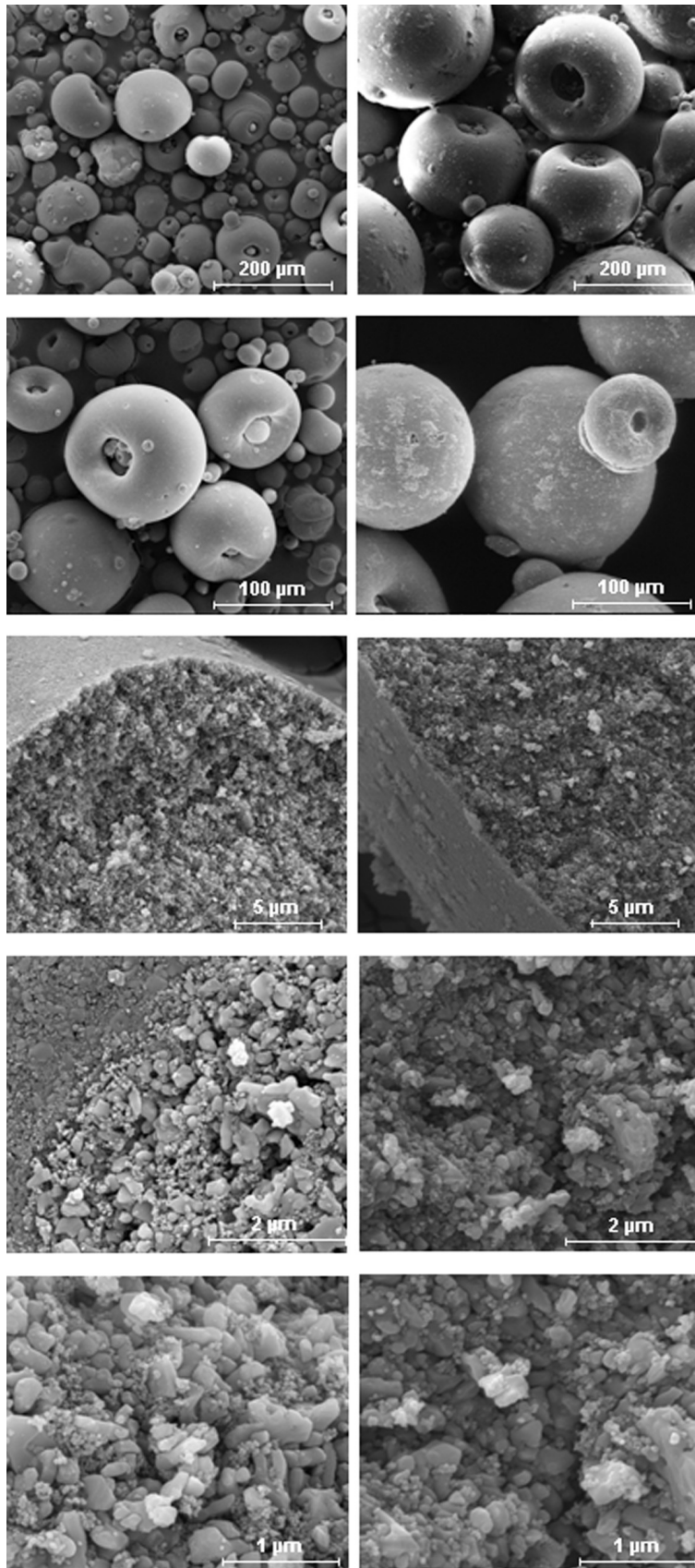
Figure 2. Shrinkage versus temperature curves for samples AsTn30 and AsTn50 together with the reference NC powder obtained by means of the hot stage microscope.
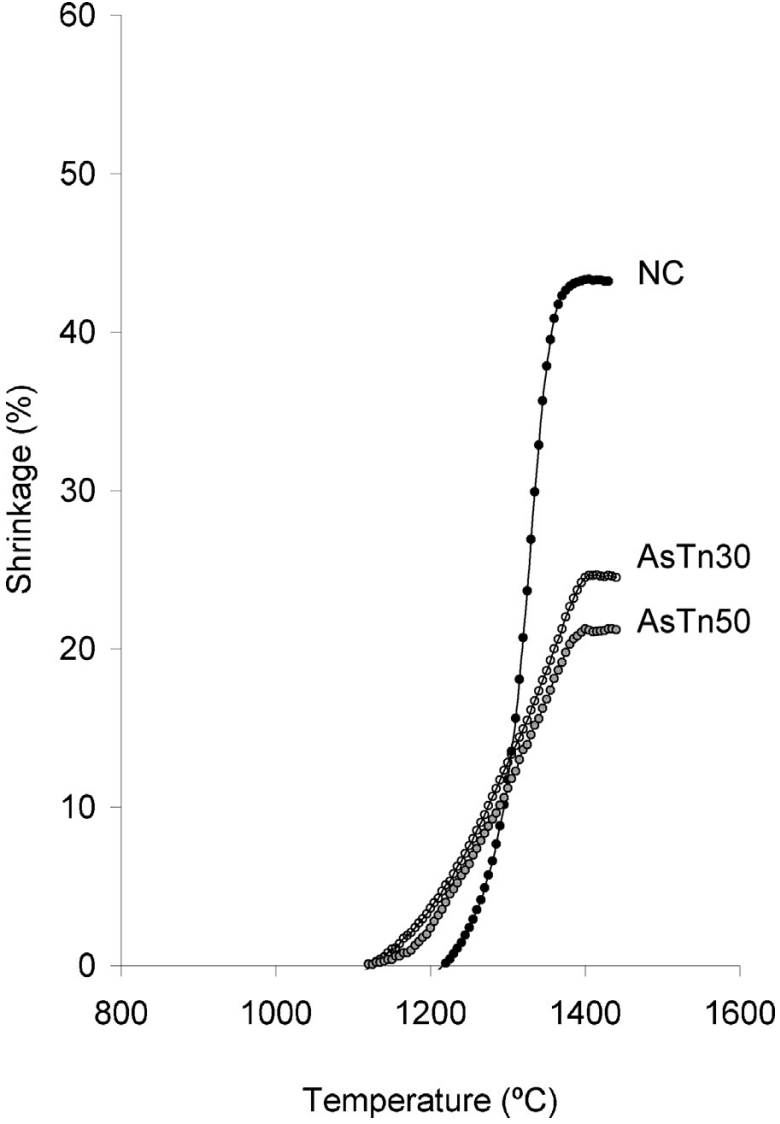
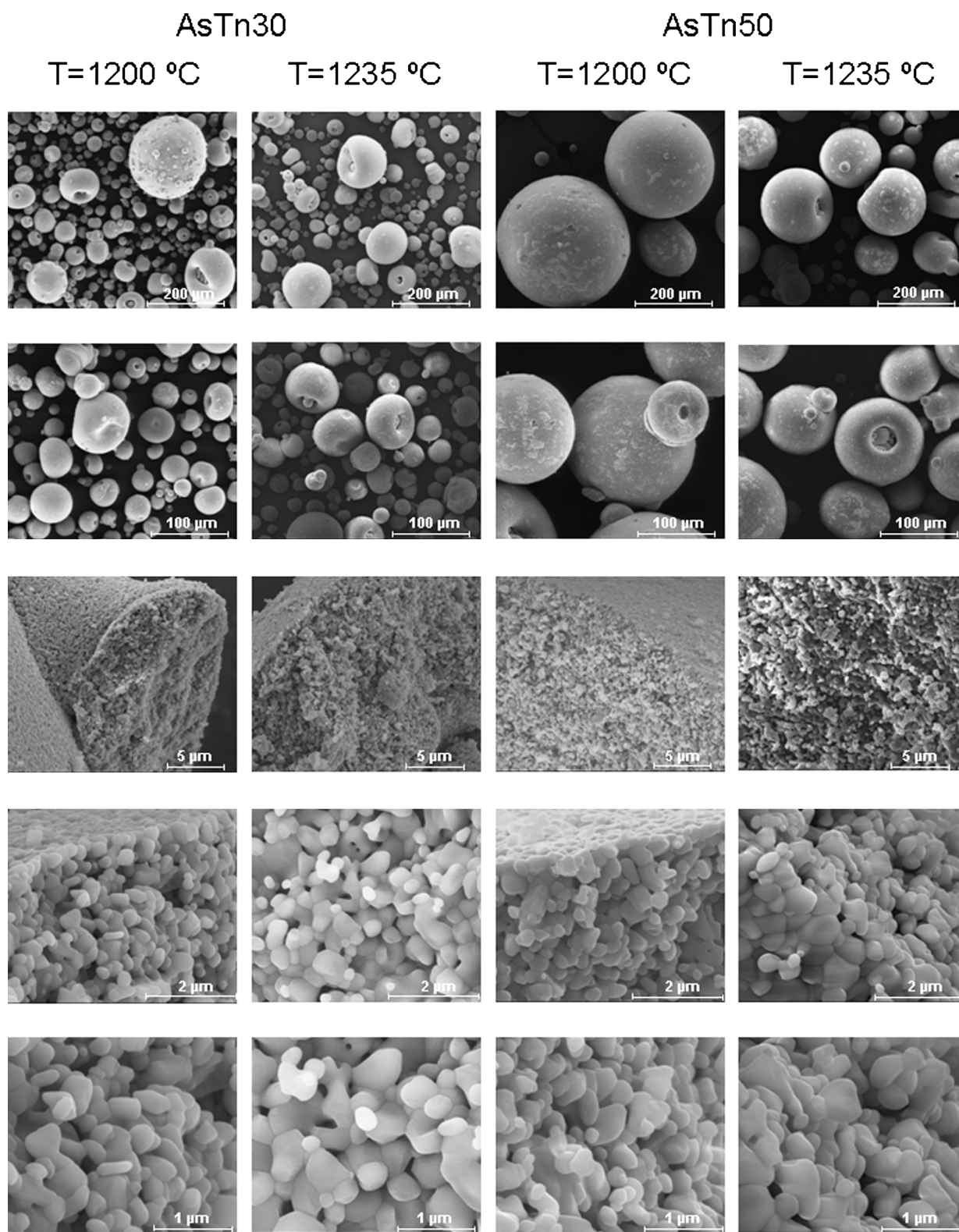Figure 3. FEG-ESEM micrographs of AsTn30 and AsTn50 spray-dried powders thermally treated at two temperatures.

Figure 4. Pore size distribution curves obtained by mercury intrusion porosimetry for AsTn30 and AsTn50 powders thermally untreated and thermally treated at 1235 ºC.
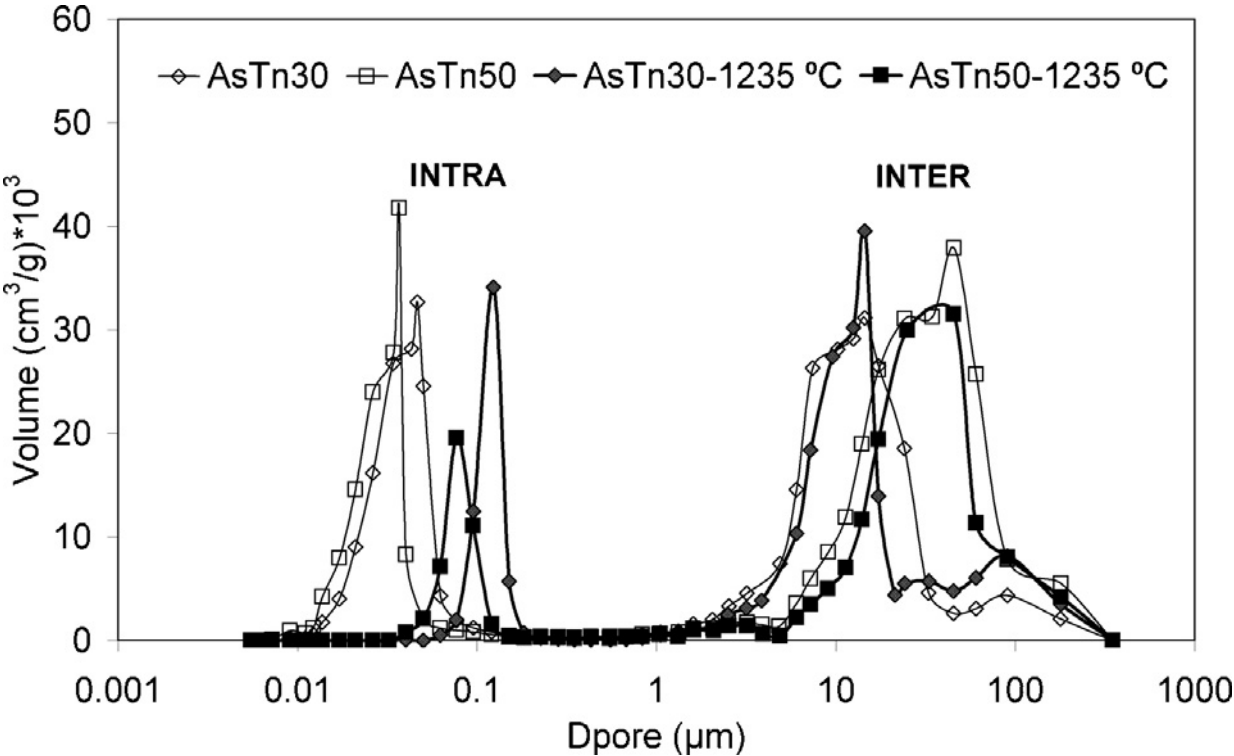
Figure 5. Granule size distribution of the thermally treated spray-dried powders obtained from 30 vol.% and 50 vol.% suspensions (samples AsTn30-1200 ◦C and AsTn50-1200 ◦C, respectively
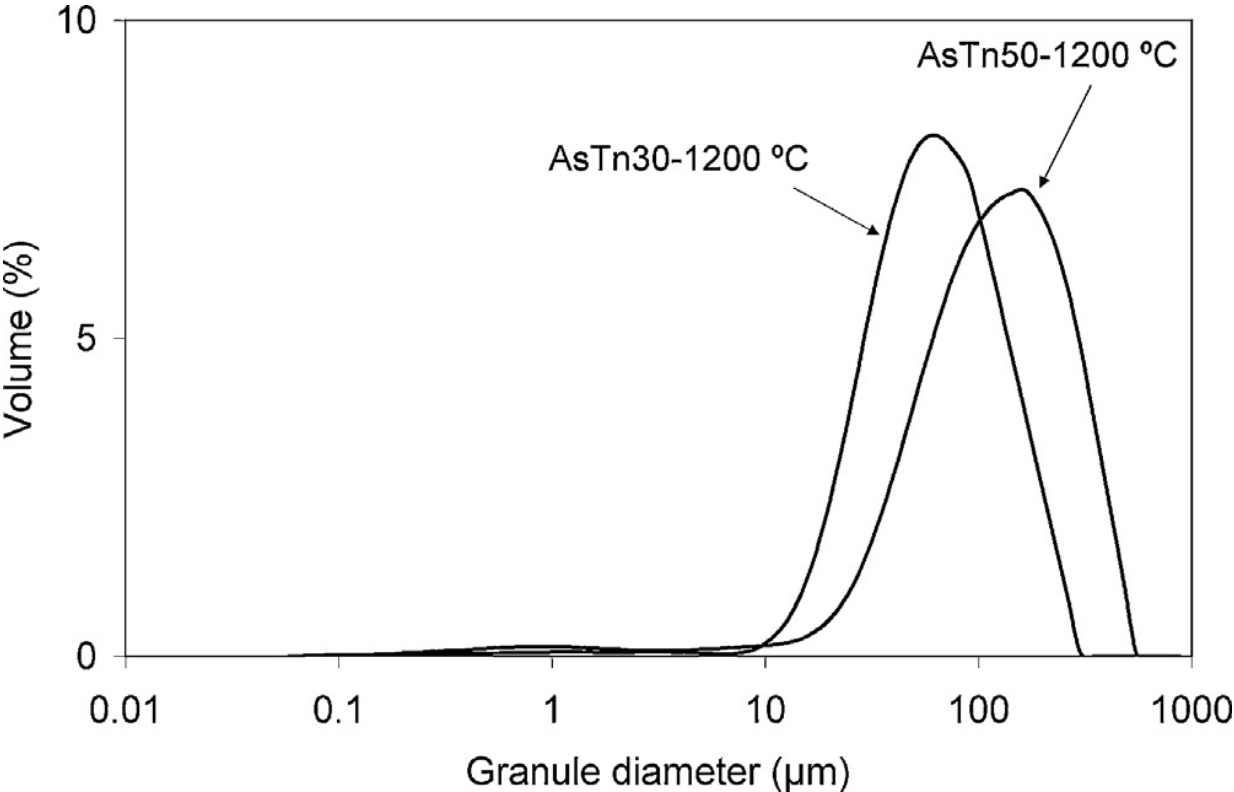
Figure 6. XRD patterns for AsTn50 powder untreated and thermally treated at 1200 ºC.
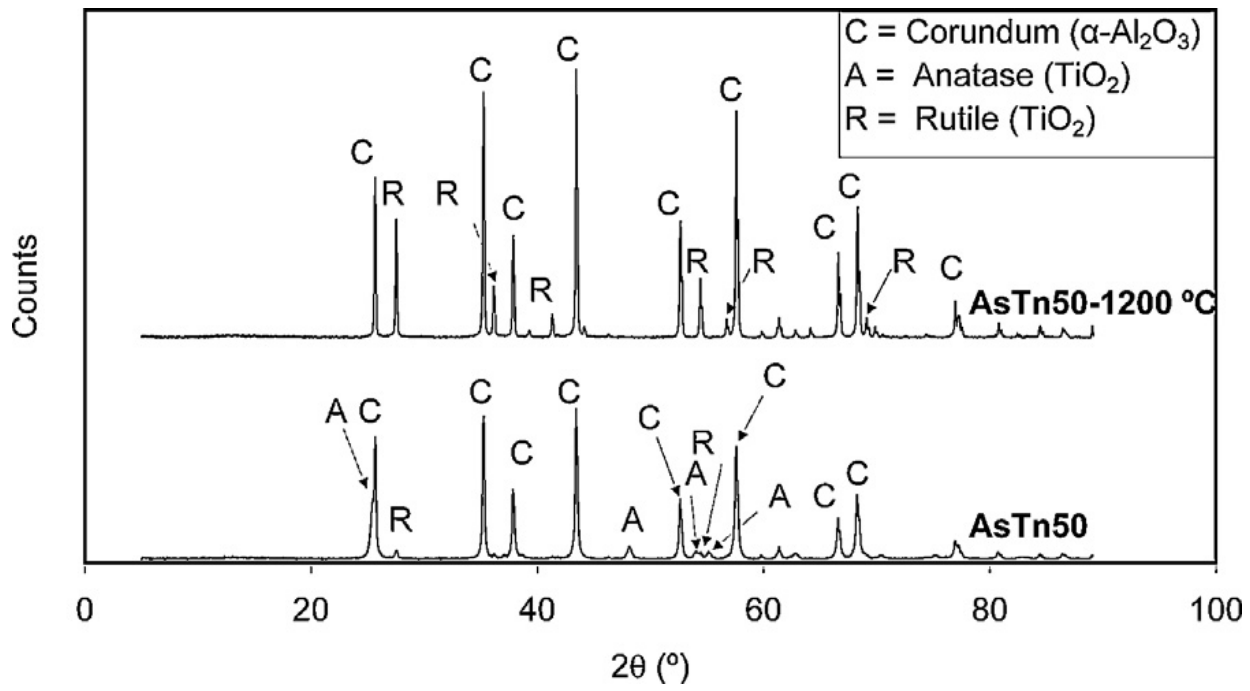
Figure 7. SEM micrographs of AsTn30, AsTn50, AsTn30-1200ºC and AsTn50-1200 ºC powders together with two representative micrographs of reference coatings (MC and NC) obtained with the same spraying conditions.
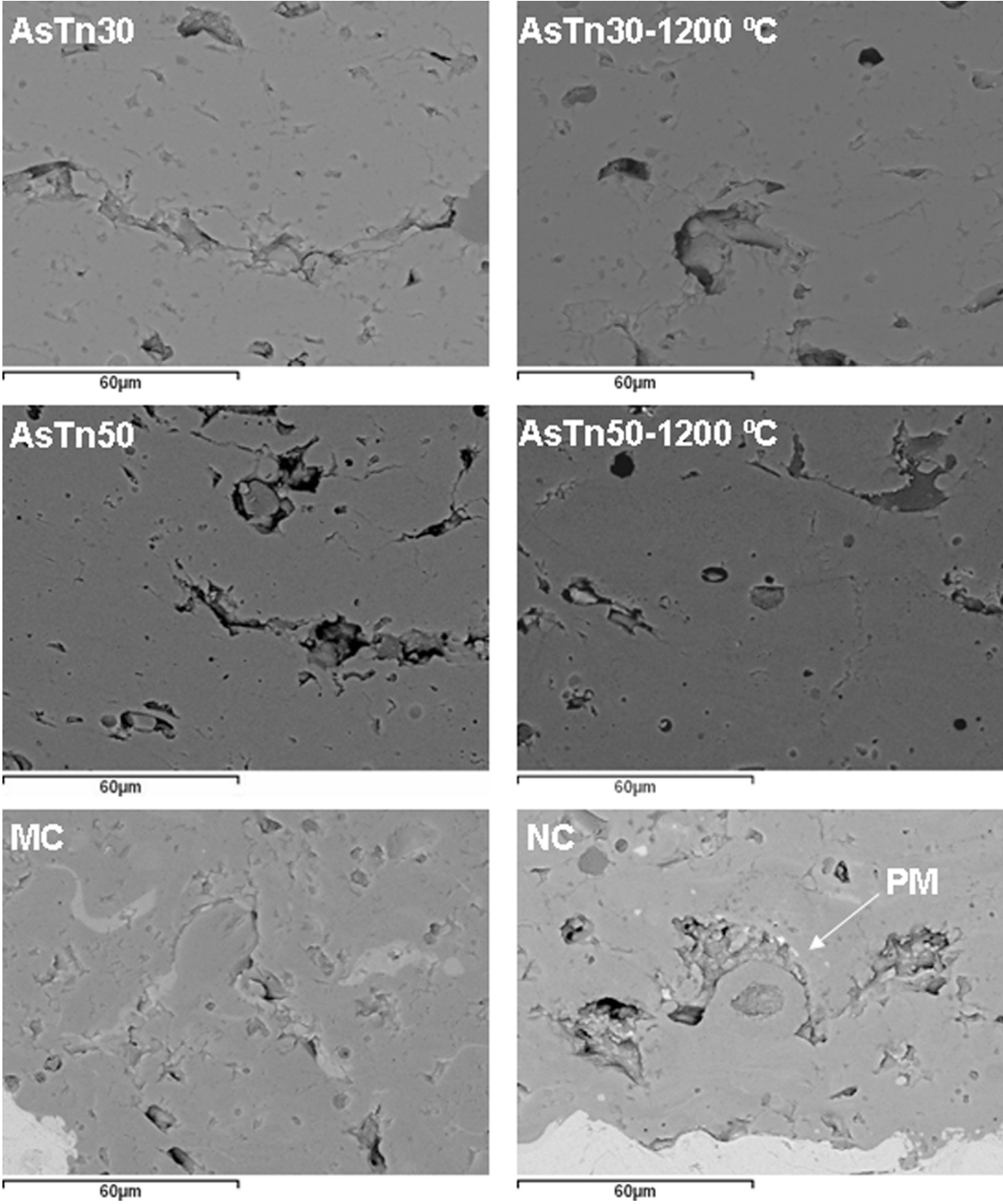
Figure 8. Comparison of higher magnification micrographs of the partially molten areas in NC and AsTn50-1200 ℃ coatings.
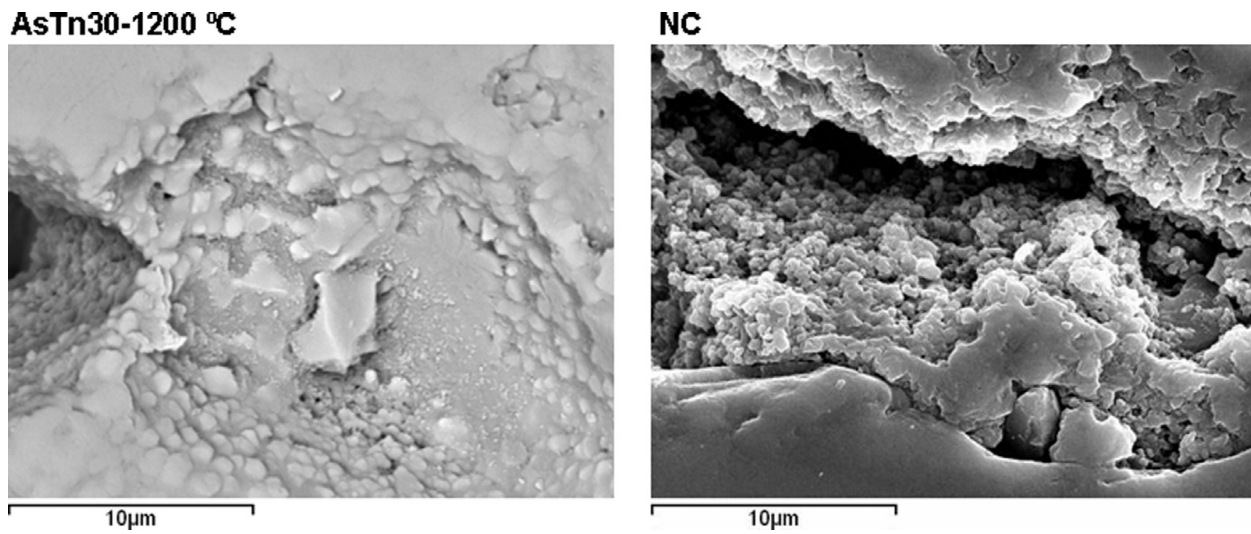
AsTn30-1200 ℃

NC

Figure 9. XRD patterns of coatings obtained from (a) AsTn30 and AsTn30- 1200 ℃ powders, and (b) AsTn50 and AsTn50-1200 ∘C powders.
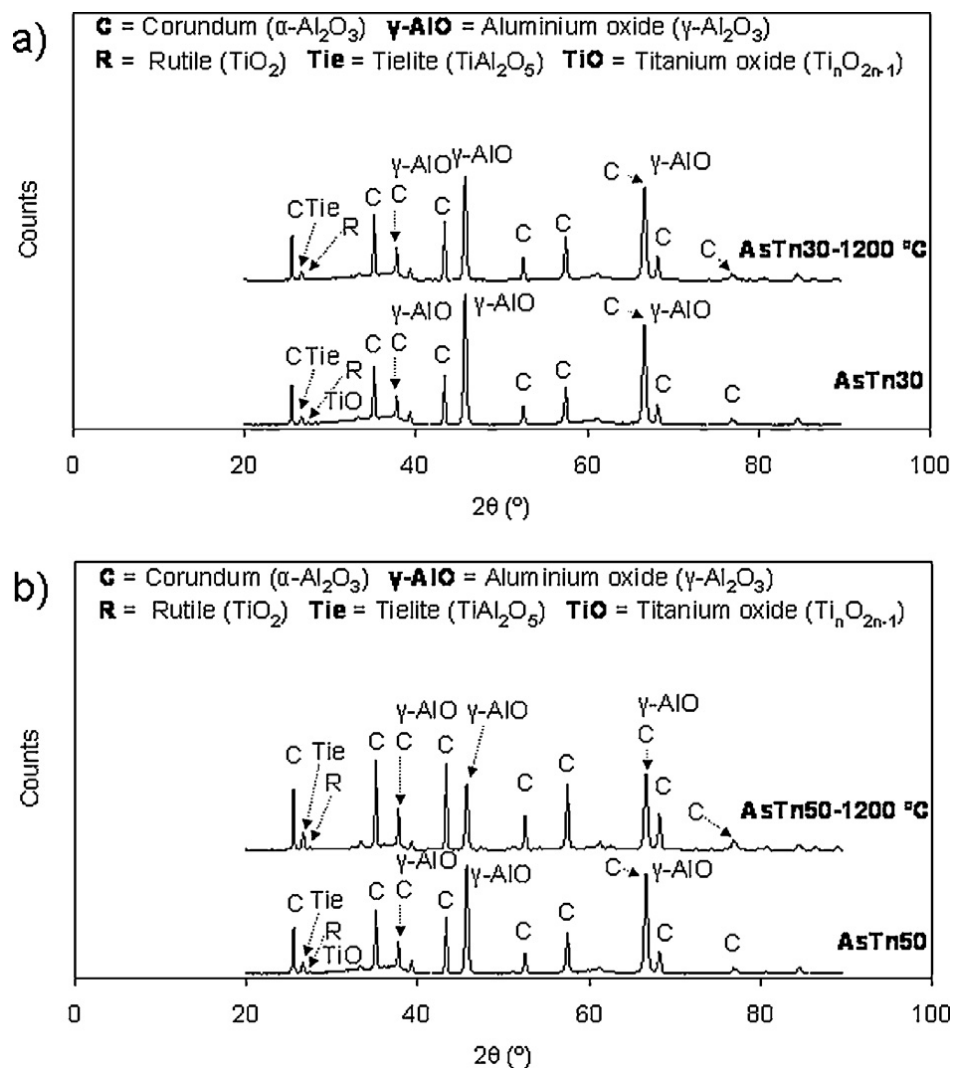
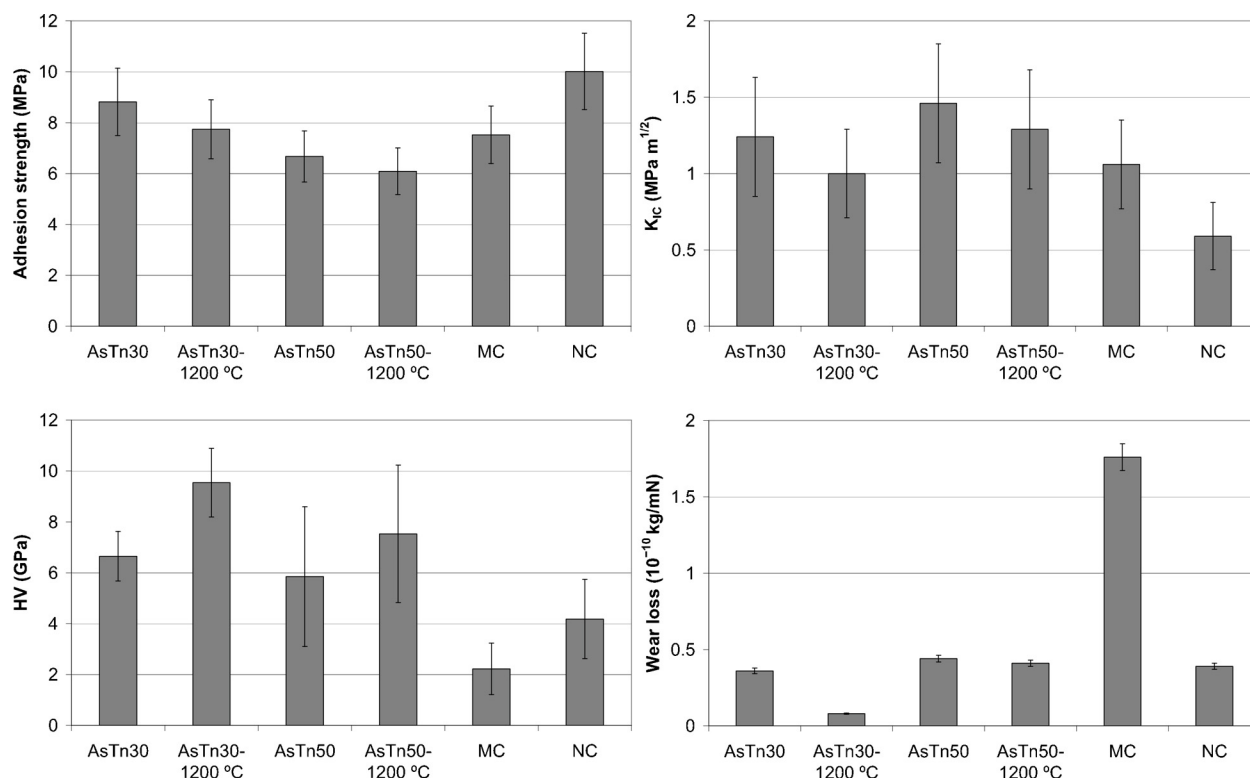Figure 10. Mechanical properties of all the coatings studied.

Table 1 Main powder characteristics of all feedstocks studied in this work.

Main powder characteristics of all feedstocks studied in this work.

Feedstock characteristics	AsTn30	AsTn50	AsTn30-1200 °C	AsTn50-1200 °C	MC	NC
Volumetric mean size (μm)	$-^a$	$-^a$	57	110	36	38
Granule bulk density (kg/m^3)	2510 ± 15	2780 ± 20	3100 ± 20	3580 ± 30	3830 ± 15	1730 ± 15
Hausner ratio	1.18 ± 0.03	1.16 ± 0.03	1.25 ± 0.03	1.18 ± 0.04	1.28 ± 0.04	1.19 ± 0.03

[a] Granule size distribution could not be measured by laser diffraction but FEG-ESEM micrographs confirm similar size in thermally untreated and in heat-treated powders.

Table 2 Microstructural features of the coatings obtained from reconstituted powders both untreated and heat treated as well as from the reference feedstocks

	AsTn30	AsTn50	AsTn30-1200 °C	AsTn50-1200 °C	MC	NC
Porosity (%)	8 ± 1	7 ± 1	5 ± 1	5 ± 1	3.0 ± 0.5	3.0±
Thickness (μm)	173 ± 16	213 ± 34	173 ± 30	170 ± 25	52 ± 14	103